SEISMIC PERFORMANCE EVALUATION OF A HORIZONTALLY CURVED HIGHWAY BRIDGE USING INCREMENTAL DYNAMIC ANALYSIS IN 3D

DIMITRIOS VAMVATSIKOS, IOANNIS SIGALAS
School of Civil Engineering, National Technical University of Athens
Iroon Polytexneiou 9, 157 80 Athens, GREECE

ABSTRACT

The seismic performance of a horizontally curved highway bridge is examined using Incremental Dynamic Analysis (IDA) in 3D. IDA has been successfully applied to two dimensional structures with a single horizontal ground motion component. An extension to three dimensions and two components of motion is needed to capture the performance of this asymmetric structure. It involves performing a series of nonlinear timehistory analyses under a suite of ground motion records, equally scaling both components of each record to several levels of intensity and monitoring the resulting structural response. The complete spectrum of structural behavior is thus recovered, from elasticity to final global instability for combinations of intensities in the two directions. Using a single intensity measure or a vector of two (e.g. spectral coordinates of the record components) and appropriate engineering demand parameters (e.g., maximum peak column drift), the familiar IDA curves plus novel IDA surfaces are created, clearly showing the bridge response and its statistical summary at any intensity level. This is a powerful, albeit resource intensive, analysis procedure that is well suited to evaluate the performance of asymmetric structures under seismic loads and may serve as a solid benchmark for evaluating the accuracy of simpler methods.

INTRODUCTION

It is common practice in earthquake engineering to analyze spatial structures using two-dimensional (2D) models and associated methods. Still, when the structure under consideration has a complex irregular geometry such schemes usually fail, resulting in the need to create and analyze full 3D models. Unfortunately, in such cases several analysis problems appear. Most work is still being done in 2D and as a result fast and inexpensive methods such as the static pushover are still being developed and tested to accurately capture 3D effects. Actually, in the past few years we have witnessed a resurgence of simplified methodologies to predict 3D structural behavior, a non-exhaustive list including the work of Moghadam and Tso [1], Fajfar [2], Penelis and Kappos, [3] and Chopra and Goel [4]. While important advances have been thus achieved, the errors inherent in any such approximating approach often reach unacceptable values, especially for performance levels close to collapse.

These limitations became quite restricting when faced with the need to evaluate the design of a horizontally curved highway bridge designated as G7 for Egnatia Odos S.A. Having a total length of 270m with a radius of curvature of only 320m plus some complex abutment-deck connection details make this an interesting asymmetric structure. One could say that this is an ideal testing ground to implement Incremental Dynamic Analysis in a 3D setting.

Incremental Dynamic Analysis (IDA) (Vamvatsikos and Cornell [5]) has recently emerged as a promising method to evaluate the performance of structures under seismic loading. It involves subjecting a structural model to a suite of ground motion records, each scaled to several intensities (as measured by the intensity measure, IM), and recording the responses (measured by engineering demand parameters, EDPs) at each level to form IDA curves of response versus intensity. Allowing for the transparent definition of limit-states and the accurate estimation of the distribution of the associated capacities, it forms a reliable computer-intensive platform for performance-based earthquake engineering. Still, while the original framework set forth by Vamvatsikos and Cornell [5] does encompass 3D applications, most studies so far have been restricted to 2D structures. Actually, applying IDA in 3D is a straightforward exercise in post-processing the results of the dynamic analyses. However it becomes quite complicated and extremely interesting when we contemplate the issue of using a vector of intensity measures, one for each horizontal component of the ground motion.

BRIDGE AND MODEL DESCRIPTION

Bridge G7 is circular in plan with a 320m radius and comprises a three span 75+120+75m continuous deck monolithically connected to piers and simply supported at the abutments (Figure 1). The prestressed concrete deck structure is a single cell box girder with depths varying from 7.25m at the piers to 2.75m towards the mid span and abutments. The box type piers M1 and M2 have outer dimensions 7.35 x 4.0m, 0.75m wall thickness and clear heights of 41.70m and 49.50m respectively. Both piers are founded on cylindrical 10m-diameter 15.0m-long solid rockshafts bearing on rock, a gabbros formation. Solid seat type abutments founded on bored piles are provided at both ends (Figure 2). Free-sliding pot bearings and a shear key are installed at the abutment support axis to restrict the deck movement in the radial direction. A pair of seismic stoppers at each abutment achieves restriction of the radial movements in case of excessive earthquake forces which cause yielding of the shear key.

The OpenSEES platform (McKenna et al [6]) was selected to form and analyze the bridge model. Being extremely flexible and robust it allows for a detailed and accurate simulation of the bridge. Thus the pier columns were modeled using a flexibility-based fiber element formulation with an exact corotational formulation to account for geometric nonlinearities (P-Δ effects). The effects of concrete confinement were modeled according to Mander et al [7] while the reinforcing bars were allowed to buckle under compression when the lateral support was inadequate. The deck was assumed to remain elastic and was represented with centerline beam-column elements that were appropriately selected to simulate the gradual changing of the cross-section. The foundations, being embedded solidly in rock, were assumed to be fixed. Finally, the abutment pot-bearings were simulated with complex multi-linear springs that include the gap between the deck and the abutment walls and the breaking of the shear key. The resulting model has a 1st mode period of 1.65s, mostly a longitudinal (x-axis) translation, and a 2nd mode period that resembles a transverse (y-axis) translation at 1.54s. In essence this is a torsionally-stiff structure as the torsional mode is not among the first two modes [2].

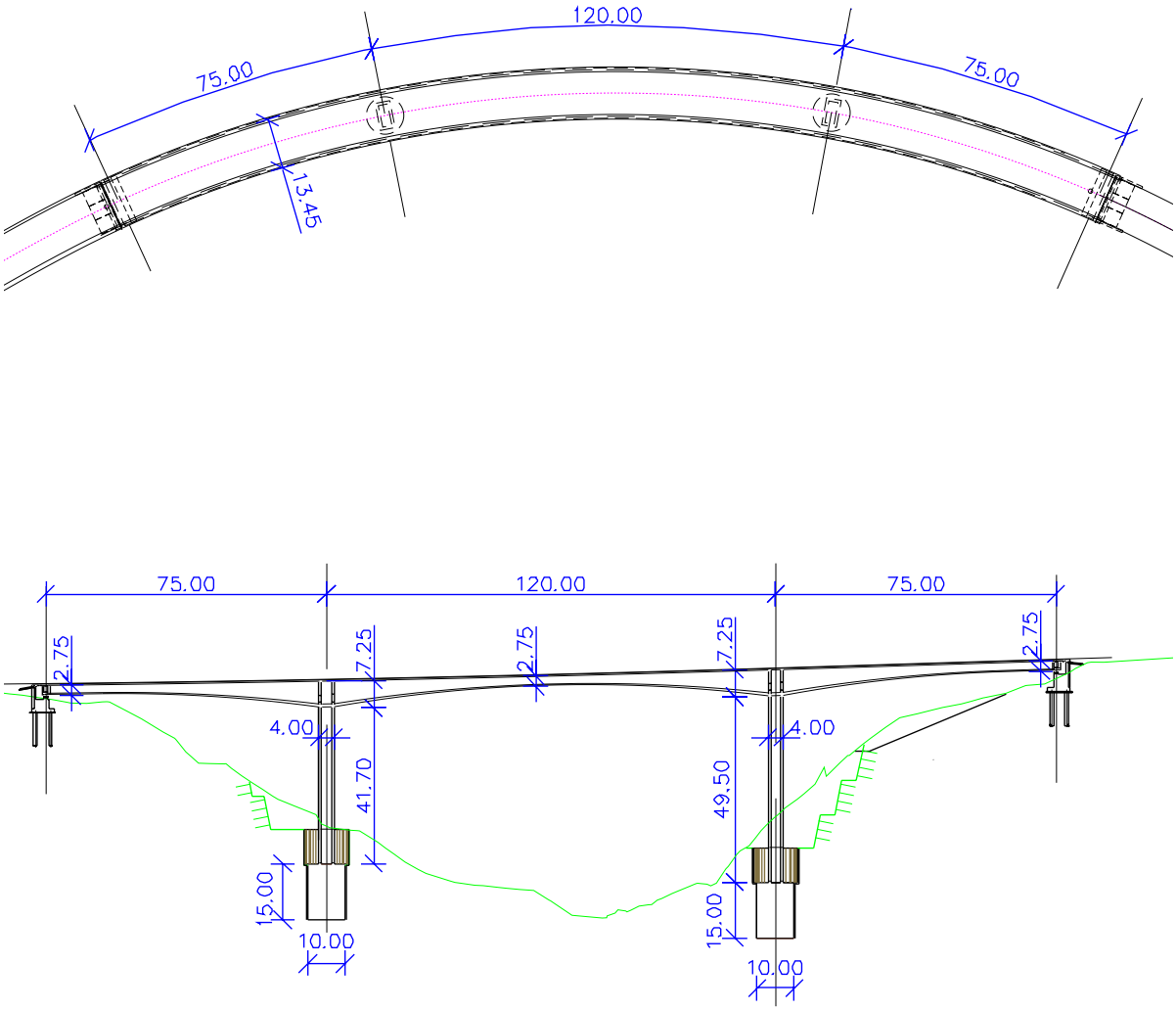

Figure 1: Plan and longitudinal-section of the bridge (all dimensions in meters).

In order to understand the behavior of the bridge we have performed static pushover analysis with force patterns that resemble the 1st and the 2nd mode of the building, or, practically speaking, for forces acting along the global x-axis and along the global y-axis separately. To record the structural response we have used θ_{max}, the maximum (over both piers) square-root-sum-of-squares (SRSS) value of the x and y column-drift values. The results appear in Figures 3a-b for the 1st and 2nd mode, clearly showing the sensitivity of the structure to translation along the longitudinal direction. The x-axis pushover reaches its maximum base shear value at a drift of about 1.5%. Then the columns start losing strength and the bridge assumes negative stiffness. At a drift of about 2.7% the deck has displaced enough so that it falls off the abutment seat. Of course the model cannot register this event so the pushover curve happily continues until the other end of the bridge hits the abutment end-wall, showing a sharp increase in stiffness. Obviously, this part of the curve should be discarded. In the y-axis pushover the bridge appears much stiffer and able to withstand much higher base shears. Naturally we should expect that the primary mode of failure for this system will be the deck falling off the abutment seat. While significant plastic hinges will have formed in the pier columns, they are much too strong to collapse before this catastrophic deck unseating occurs.

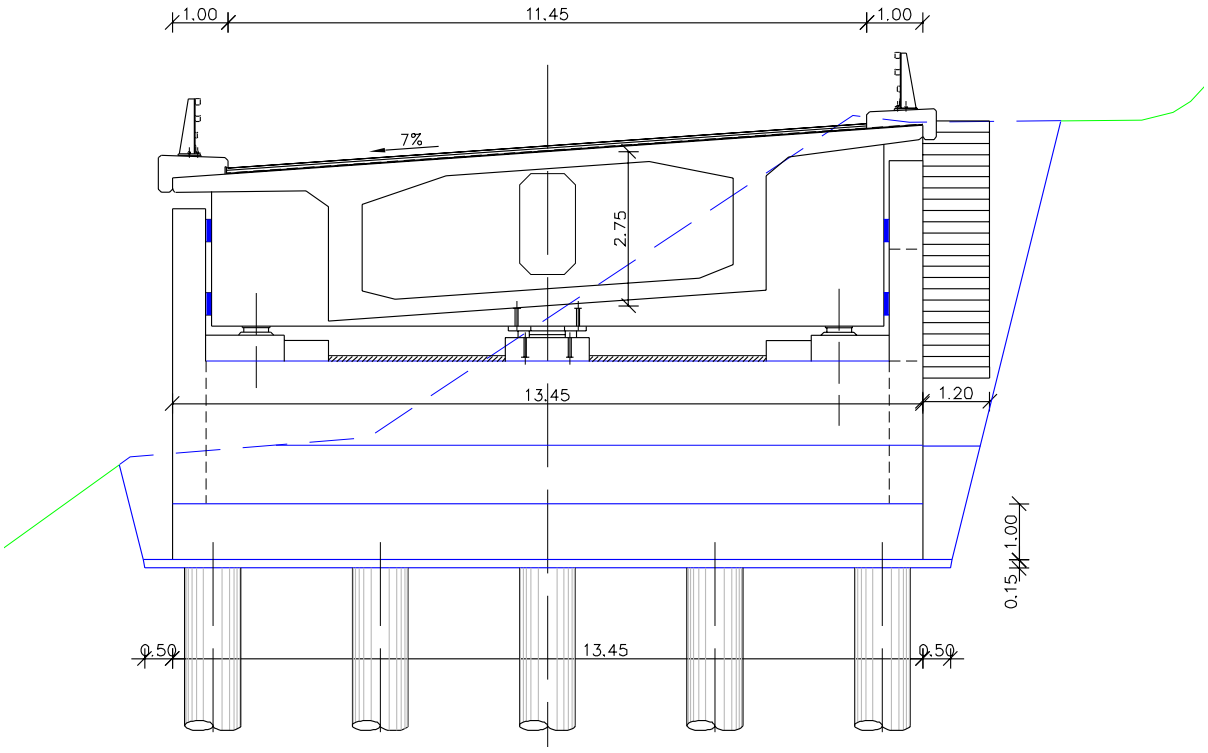

Figure 2: Abutment – bridge connection details (all dimensions in meters).

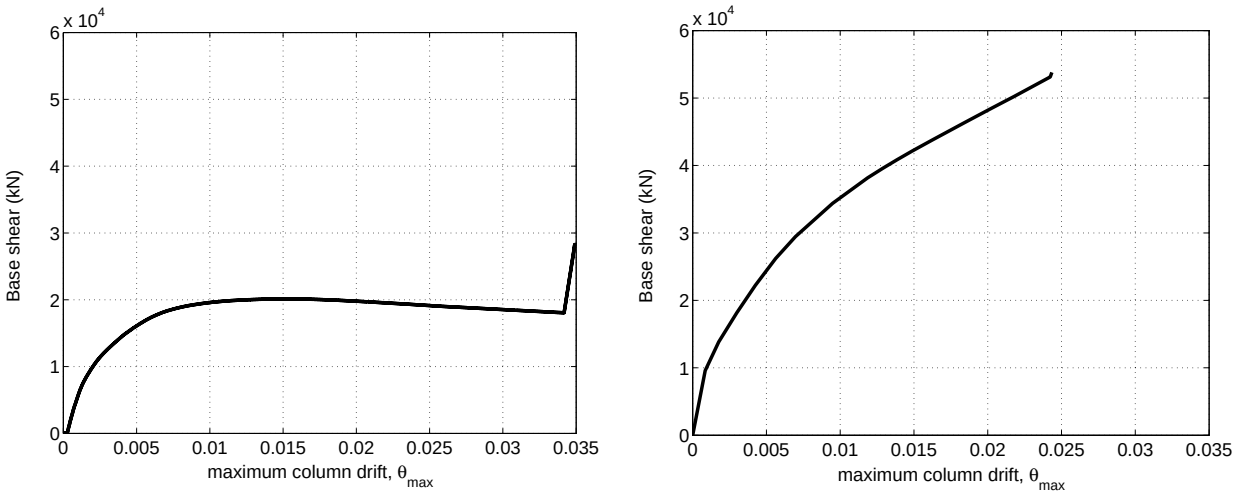

Figure 3: Pushover curves for (a) 1st mode (*x*-axis) and (b) 2nd mode (*y*-axis) force patterns.

Recently proposed pushover schemes for evaluating the 3D behavior of this structure would require combining these pushovers, either via an SRSS rule (Fajfar [2]) or by the appropriate modal contribution factors (Chopra and Goel [4]). Of course these methods are approximate and there may be doubts regarding their performance in a dynamically complex setting. There are several arguments against or in favor of the adequacy of such methods for this bridge. First of all the structure is well approximated by a single-degree-of-freedom system. On the

other hand, this system would have to be quite complex because of the bridge details. Most important is the fact that there is a gap-stopper system acting in the radial direction for each abutment. There are several interesting dynamic phenomena that appear in such cases which may are far from the realm of simple elastoplastic systems used to derive most *R-μ-T* relationships. There is also the issue of the shear keys that restrain radial displacements at the abutments and initially stiffen the transverse mode to 1.54s; when they break (which by design happens quite early) they cause a period jump to about 2.3s. Such issues often appear when performing pushover on any irregular or unusual system and there will remain a continuing need to verify its accuracy. We will not proceed to actually settle this argument, but we do aim to provide a solid method that can become the standard in evaluating 3D structures and serve as a benchmark to rate the adequacy of simpler schemes.

PERFORMING IDA FOR 3D STRUCTURES

Performing IDA on a structural model requires a suite of ground motion records to represent the seismic threat, an efficient intensity measure (IM) to scale the records and an appropriate choice of engineering demand parameters (EDPs) to adequately characterize the structural response. All three elements are necessary ingredients of IDA and perhaps the most important difference in selecting them when doing 3D versus 2D analysis is that we now need two components of ground motion instead of just one.

Therefore, we are going to use thirty ground motion records with two horizontal components, shown in Table-1. These were selected from a relatively narrow magnitude and distance bin, having moment magnitude within 6.5 – 6.7 and closest distance to fault rupture ranging from 13.3 to 31.7km. They have all been recorded on firm soil and bear no marks of near-fault directivity, generally putting them in the "regular" ground motion category.

What is truly important in selecting an IM for the scaling of the records is getting good correlation with collapse and a relatively low dispersion in the collapse IM-values (the flatlines) so that the IDA curves are traced efficiently (Vamvatsikos and Cornell [8]). A mediocre choice is not a problem when using high-performance IDA-tracing algorithms like *hunt & fill* [8], but a very poor IM-choice may increase the number of runs required to get a reasonable resolution. Since the G7 bridge is quite sensitive to longitudinal translations, i.e., in the first-mode, the longitudinal (*x*-axis) ground motion component should govern collapse. Therefore we choose as our IM the 5%-damped first-mode spectral acceleration of the *x*-axis component, $S_{ax}(T_1,5\%)$. Note that this choice will not restrict us in any sense when post-processing the results. It need only be used for the scaling of the records when performing IDA and may later be replaced by any other scalable IM [8]. Actually, this is a quite good IM-choice after all and using the *hunt & fill* algorithm allows the use of only 8 runs to accurately capture the IDA curve for each ground motion.

Selecting the EDPs is an exercise in understanding which elements of the bridge sustain damage from earthquakes and their performance determines a limit-state, e.g., rendering the bridge inoperational by necessitating repairs or even inspection. In our case these are the abutment bearings and the piers. Any limit-state definition needs to take into account limiting values for both of them. In specific for the bearing we need to keep track of the "positive" bearing displacement $d^{+}_{x,\max}$, defined as the displacement away from the bearing seat. This measures exactly the separation between the deck and the abutment; if it exceeds 1.0m it will

result in deck unseating. Additionally it is useful to monitor the maximum peak bearing uplift, $d_{z,\max}$, excessive values always being a concern in bridge design. Regarding the pier columns we need to at least track the maximum peak SRSS drift $\theta_{\max}$, which correlates well with column damage. In total we have selected three different EDPs, all of which can play a part in defining limit-states. Now all we have to do is run the nonlinear dynamic analyses and each time recover and record the EDPs for post-processing.

Table-1: The suite of thirty ground motion records (two components each) used. First component (1) is applied along the *x*-axis and the second (2) along the *y*-axis of the model.

Event Station	R [1] Km	Soil [2]	φ_1 [3] Deg	φ_2 [3] deg	PGA_1 g	PGA_2 g
Superstition Hills 1987 (M=6.7) [4]						
1. Plaster City	21.0	C,D	135	045	0.12	0.19
2. Brawley	18.2	C,D	225	315	0.16	0.12
3. Wildlife Liquef. Array	24.4	–,D	090	360	0.18	0.21
4. Westmoreland Fire Station	13.3	C,D	090	180	0.17	0.21
5. El Centro Imp. Co Cent	13.9	C,D	000	090	0.36	0.26
San Fernando, 1971 (M=6.6)						
6. LA Hollywood Sto Lot	21.2	C,D	090	180	0.21	0.17
Imperial Valley 1979 (M=6.5)						
7. Chihuahua	28.7	C,D	012	282	0.27	0.25
8. Plaster City	31.7	C,D	045	135	0.04	0.06
9. Compuertas	32.6	C,D	015	285	0.19	0.15
10. El centro Array #12	18.2	C,D	140	230	0.14	0.12
11. El centro Array #13	21.9	C,D	140	230	0.12	0.14
12. Westmoreland Fire Station	15.1	C,D	090	180	0.07	0.11
13. El centro Array #1	15.5	C,D	140	230	0.14	0.13
Northridge 1994 (M=6.7)						
14. Leona Valley #2	37.7	C,–	000	090	0.09	0.06
15. Lake Hughes #1	36.3	C,C	000	090	0.09	0.08
16. LA Hollywood Sto FF	25.5	C,D	090	360	0.23	0.36
17. LA Baldwin Hills	31.3	B,B	090	360	0.24	0.17
18. Canoga Park - Topanga Can	15.8	C,D	106	196	0.36	0.42
19. LA N Faring Rd	23.9	C,B	000	090	0.27	0.24
20. LA Fletcher Dr	29.5	C,D	144	234	0.16	0.24
21. LA Centinela St	30.9	C,D	155	245	0.47	0.32
22. Glendale Las Palmas	25.4	C,C	177	267	0.36	0.21
Loma Prieta 1989 (M=6.9)						
23. Hollister Diff Array	25.8	–,D	165	255	0.27	0.28
24. WAHO	16.9	–,D	000	090	0.37	0.64
25. Halls Valley	31.6	C,C	000	090	0.13	0.10
26. Agnews State Hospital	28.2	C,D	000	090	0.17	0.16
27. Anderson Dam Downstrm	21.4	B,D	270	360	0.24	0.24
28. Coyote Lake Dam Downstrm	22.3	B,D	195	285	0.16	0.18
29. Sunnyvale Colton Ave	28.8	C,D	270	360	0.21	0.21
30. Hollister South & Pine	28.8	–,D	000	090	0.37	0.18

[1] Closest distance to fault rupture
[2] USGS, Geomatrix soil class
[3] Component
[4] Moment magnitude

POSTPROCESSING WITH A SCALAR INTENSITY MEASURE

Each analysis produces several pairs of intensity versus response values. These are points in the IM-EDP plane which can be interpolated with a flexible spline scheme [8] to produce thirty IDA curves for each EDP. Figure 4a shows the resulting IDA curves for the deck-abutment separation $d^{+}_{x,\max}$. When these reach 1.0m, a flatline occurs, as the deck has fallen off and the bridge is now considered to have collapsed. These flatlines set the maximum IM limit that the design can withstand and they are the same (in IM terms) for all EDPs. Observe the wide dispersion these curves have, practically at any level of intensity and any limit-state. For some records collapse occurs for $S_{ax}(T_1,5\%)$ as low as 0.7g while for one record deck un-seating appears at intensities in excess of 4g.

Summarizing the IDA curves to produce the distribution of EDP demands given the IM value is straightforward. By calculating cross-sectional fractiles of the EDP at each level of intensity we can calculate the 16, 50 and 84% fractile IDA curves. In Figure 4b appear the fractile curves for $d^{+}_{x,\max}$, showing, for example, that 84% of the records will cause collapse when scaled to 2.1g, 50% of the records will do so at 1.8g while 16% of them can cause collapse for values as low as 1.4g. Figures 5a and 5b contain the corresponding curves for the column drift $\theta_{\max}$ and the bearing uplift $d_{z,\max}$. Therein we can see that when close to collapse the structure will show in a median sense about 4% pier drift and sustain 3cm of bearing uplift.

In all cases though there is a considerable dispersion, in the order of 30%, even with this reasonable choice for an IM. But there is also another angle that we have not yet explored, namely the transverse component of seismic loading. We have not taken into account the intensity of the *y*-axis component of the ground motion, which may well account for some of the observed record-to-record variability. This requires the introduction of a secondary IM to form a vector of two and will be the topic of the following section.

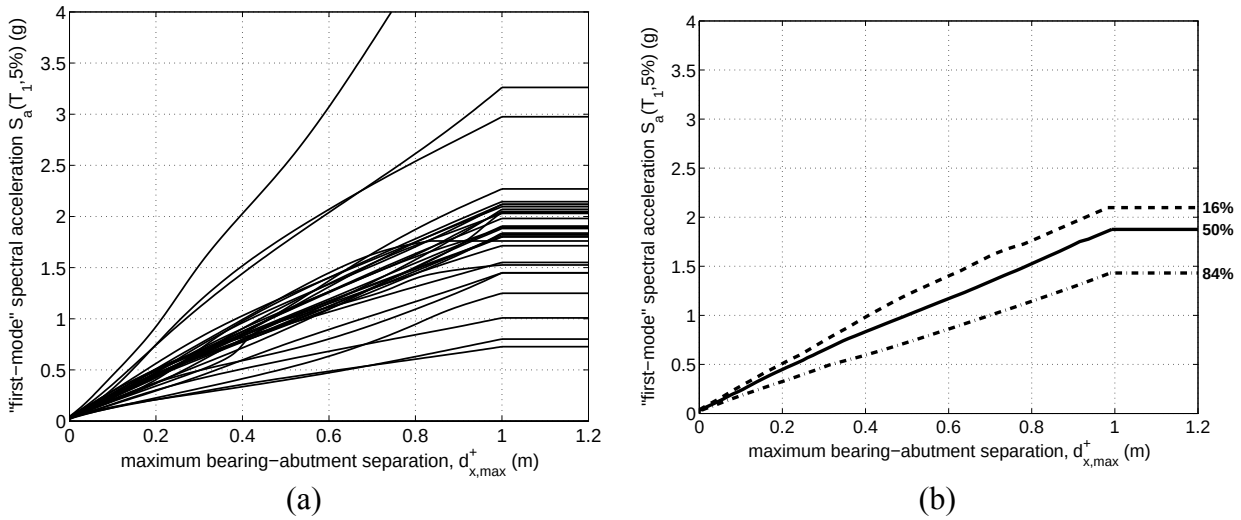

Figure 4: (a) Thirty IDA curves for the maximum bearing-abutment separation and (b) the corresponding 16, 50 and 84% fractiles.

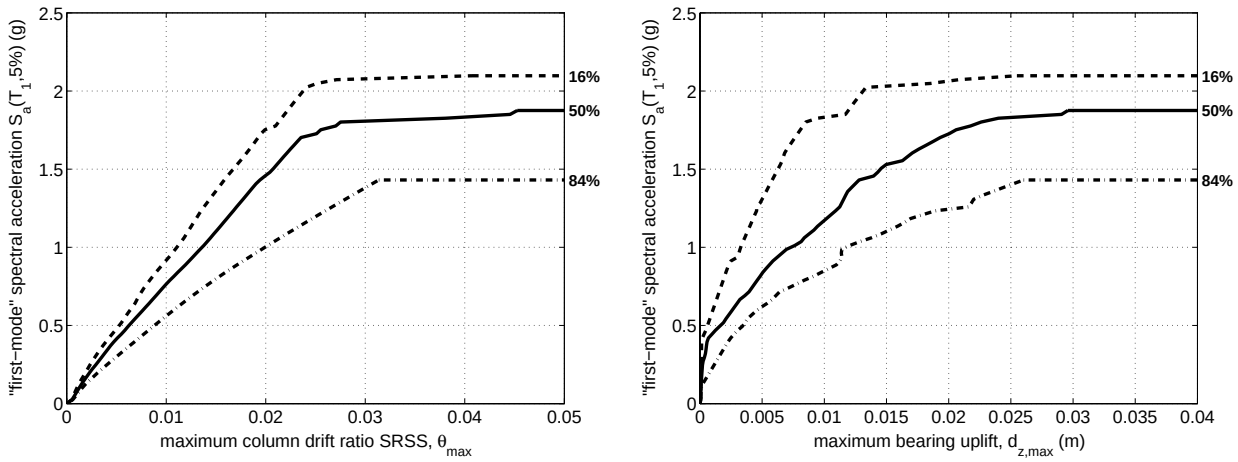

Figure 5: The 16, 50 and 84% fractile IDA curves for (a) the maximum SRSS column drift ratio and (b) the maximum bearing uplift.

POSTPROCESSING WITH A VECTOR OF TWO INTENSITY MEASURES

The use of a vector of two IMs, one for each component, does not mean that we need to rerun the dynamic analyses. Only a somewhat different post-processing is required, as explained in reference [8]. Actually the definitions set forth in [5] do provide for a vector IM, while an appropriate framework has been developed on how to post-process and summarize such data by Vamvatsikos and Cornell [9]. To facilitate understanding we will take the reader through a detailed walkthrough of all the necessary steps.

There is a single important issue when selecting a secondary IM to complement our primary choice and form a vector of two. Since the scaling is represented by the primary IM, say $S_{ax}(T_1,5\%)$, it would be redundant and often confusing if the secondary IM were also scalable rather than scaling-independent. That is not to say that one may not use another spectral value, but rather that it would be better if we normalized it by the primary IM to remove any redundant information. So we let our second IM be $S_{ay}(c\cdot T_2,5\%)/S_{ax}(T_1,5\%)$ where the subscripts "*x*" and "*y*" refer to the *x* and *y* axis component (longitudinal and transverse) and *c* is a factor used to scale the second-mode period T_2. Thus, we convey only the additional information that the new element in the vector brings in with respect to our primary scalable IM.

Following a similar procedure as for a single scalable IM, we use splines to interpolate the discrete IDA runs for each record versus the scalable IM from the vector [5]. We can then visualize the IDA curves versus the vector IM by plotting the EDP and the two single IMs in a 3D plot. In this case we will put the IMs on the *x* and *y* axis (representing the input) and place the EDP on the z-axis (since it is the response). The results for $d^{+}_{x,\max}$ and for $S_{ay}(T_2,5\%)/S_{ax}(T_1,5\%)$ as the secondary IM (c = 1.0) appear in Figure 6a. It is interesting to note that the flatlines now extend upwards, parallel to the *z*-axis, rather than being horizontal as before (Figure 4a).

Summarizing the IDA curves cannot be performed with the cross-sectional fractiles at given levels of the vector, as we did for single IMs. That would require several values of EDP at each level of the non-scalable IM, practically impossible with a limited number of records. We can use instead the symmetric-neighborhood running fractiles (Hastie and Tibshirani [10]) with a given window length to achieve the same purpose. The window length can be chosen by adopting a reasonable fraction of the sample size. In our case, we selected 30% of the sample size, i.e., we used the $0.3 \times 30 = 9$ symmetrically closest records to approximate the fractile value for each level of the non-scalable IM. The results are fractile IDA surfaces, rather than lines. For example, Figure 6b shows the median surface corresponding to the IDA curves of Figure 6a.

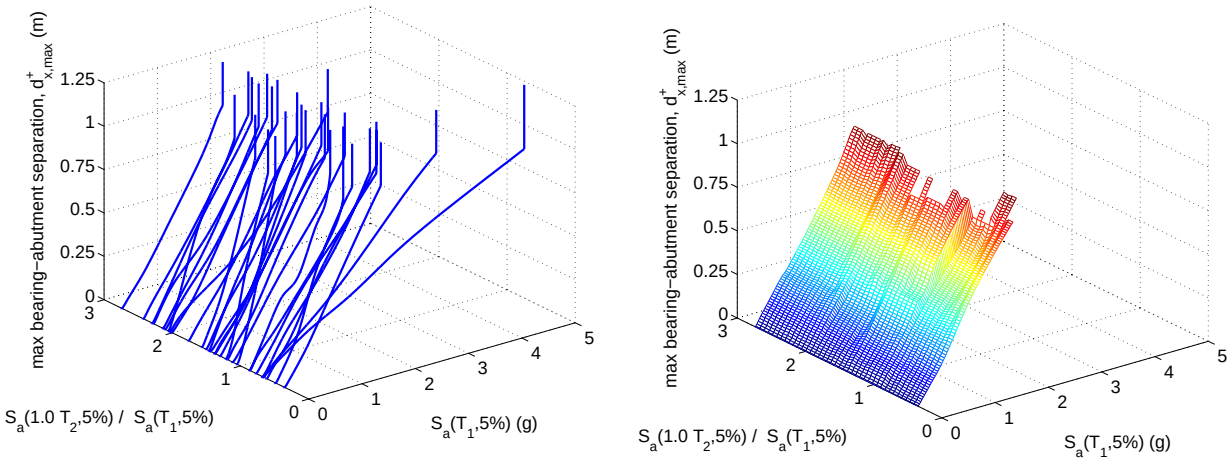

Figure 6: (a) Thirty distinct IDA curves for the maximum deck – abutment separation versus a vector IM and (b) the corresponding median IDA surface.

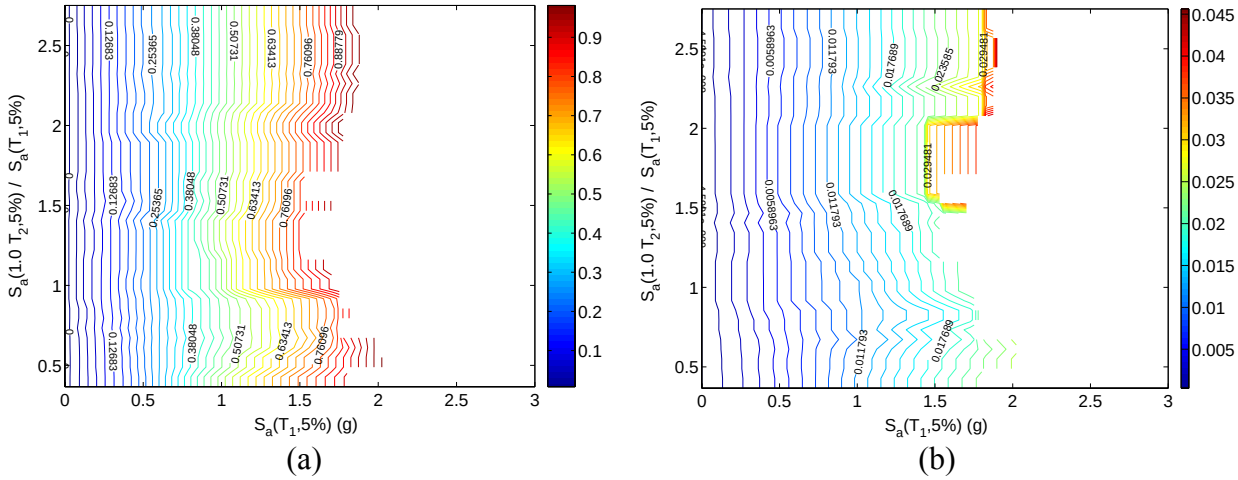

Figure 7: The median contours when c = 1.0 for (a) the maximum deck – abutment separation and (b) the maximum SRSS column drift ratio.

Now is the time to define limit-state capacities. It can be easily done using the same method as in 2D IDA curves. For example, for a limit-state at a specific EDP value (an EDP-based rule) we only need to find the vector IM values for the given value of the EDP. Simply imagine a horizontal plane (perpendicular to the *z*-axis) in Figure 6a at the given EDP-value, cutting the IDA curves to produce 30 distinct capacity points. These can be summarized in the same way as the demands, using running fractiles to compute fractile capacity *lines*. Taking advantage of the established property that the *a*% fractile of IM|EDP is equal to the (100-*a*)% fractile of EDP|IM [8] we can also perform the same operation in an indirect way by taking advantage of the fractile IDA surfaces. Imagine now horizontal planes, each for a given EDP-value, cutting the IDA surface of Figure 6b. The results can be easily visualized as contours of the fractile IDA surface, seen in Figure 7a-b for the median IDA capacities given $d^{+}_{x,\max}$ and $\theta_{\max}$, respectively.

Unfortunately, as we can see in Figure 7, little has been gained by introducing a secondary IM at the second-mode period T_2 of the *y*-component of the ground motion. Little or no dispersion has been explained by the secondary IM. This means that, practically speaking, it makes no difference whether the y-component has a relatively high spectral value at the period T_2 or not. The IM-capacities at all limit-states are going to be roughly the same in the median sense. In this case, introducing a vector IM instead of a scalar one makes no difference.

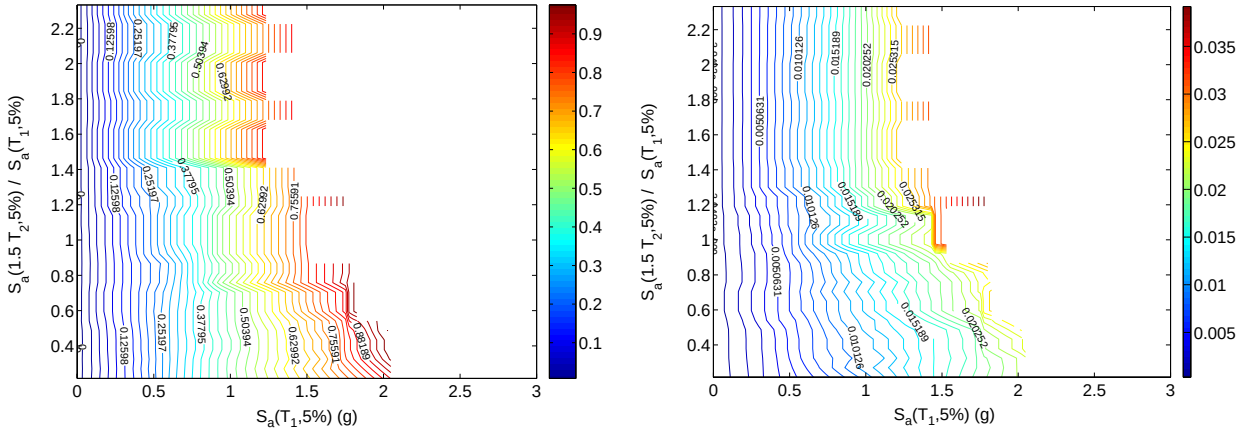

Figure 8: The median contours when c = 1.5 for (a) the maximum bearing – abutment separation and (b) the maximum SRSS column drift ratio.

On second thought we should have foreseen that. We know that the shear key in the abutments restricts the transverse bridge modes but only for low displacements. At any reasonable seismic loading this restraint is effectively removed thus freeing up the bridge considerably along the *y*-axis. Then, the transverse mode period jumps to about 2.3sec, or $1.5T_2$ which may be a much better place to look for a promising spectral value for the *y*-axis component. Actually, the calculations where repeated for this case and the results appear in Figs. 8a-b. Now the contours are much more interesting. It is obvious that a high spectral ratio, i.e., a relatively high spectral acceleration at $1.5T_2$ for the *y*-component of the earthquake has a severely negative effect for our structure. When the spectral ratio reduces from 2.0 to 0.4 we see almost an 80% improvement in $S_{ax}(T_1, 5\%)$ capacity at almost any limit-state (or EDP-level).

To further explain the meaning of these results, we are showing in Figures 9a-b the 16%, 50% and 84% capacity lines for limit-states at $d^{+}_{x,\max} = 0.7\,\text{m}$ (severe damages), and $d^{+}_{x,\max} = 1.0\,\text{m}$ (deck unseating). These correspond to our best estimate of the 16%, 50% and 84% vector IM-value of the limit-state capacity for each limit-state. For example, if several records had a spectral ratio $S_{ay}(1.5T_2, 5\%) / S_{ax}(T_1, 5\%) = 1$, in order to have the deck drop off the abutment (Figure 9b) for 16% of these records, we would need to scale both components so that $S_{ax}(T_1, 5\%) = 1\,\text{g}$. If we scale to 1.7g instead, then 50% of the records will cause collapse while it takes a scaling to 2g to reach collapse for 84% of them. On the other hand, if the spectral ratio is as low as 0.4, then these scaling levels become much higher, reaching 1.8g, 2.1g and 3.2g respectively. At the other end of the spectrum, for spectral ratios higher than one, little or no differences are observed with respect to the secondary IM. It seems that a comparatively weak y-component does indeed delay collapse, but a much stronger one will only facilitate it up to a certain limit. Since the mode of collapse is primarily *x*-axis related (longitudinal displacements causing the deck to fall of the abutment), what the *y*-component seems to mostly do is weaken the pier columns somewhat to allow for an easier extraction of the deck from the abutment. For this bridge the longitudinal component remains the primary cause that drives collapse, while the transverse component is simply assisting when it is strong enough.

As a final note, it is important to observe how we were forced to introduce summarization over windows rather than stripes. By introducing a secondary IM, we may have explained some of the variability in the capacities but we have also increased the dimensionality of the sample space, thus the data is sparser. Where we used to have 30 points for each level (stripe) of the scalable IM, we now have only a few points for whole regions of the unscalable IM.

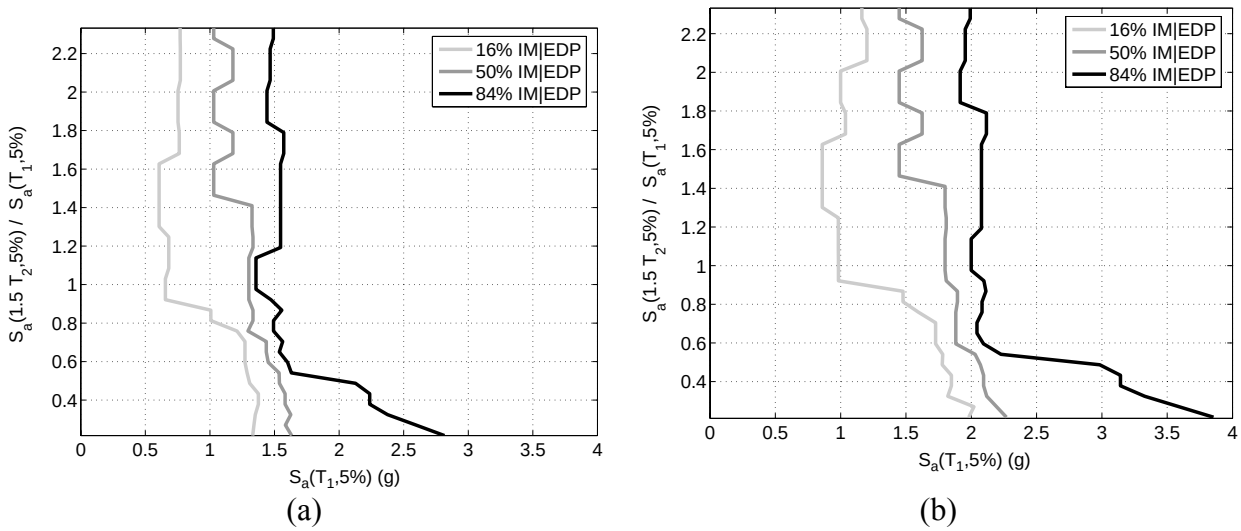

Figure 9: The 16, 50 and 84% capacity lines when *c* = 1.5 for maximum bearing – abutment separation equal to (a) 0.7m (severe damage) and (b) 1.0m (collapse).

CONCLUSIONS

The seismic performance of a horizontally-curved highway bridge has been evaluated using Incremental Dynamic Analysis in three dimensions with two components of ground motion. It has proven to be a straightforward extension of the standard 2D IDA procedure that becomes highly interesting when a vector of two IMs, one for each component of the ground motion, is used instead of a single scalar. Then, through some careful post-processing, intriguing IDA fractile surfaces and IDA capacity lines can be produced that contain unique information about the behavior of the structure. Specifically, it was found that the breaking of the shear key and the resulting increase in the transverse period of the bridge plays a major role in its dynamic response. Simply including in the vector IM the spectral value of the transverse component of ground motion at the increased period explains much of the dispersion observed in the IDA results. Interestingly enough, while a weak transverse component seems to delay collapse, a much stronger one cannot accelerate it beyond a certain point. All in all, this is a very promising methodology that can accurately quantify the seismic behavior of complex spatial structures and uncover its unique features, decisively adding to current engineering intuition.

REFERENCES

[1] Moghadam A.S., and Tso W.K. (2000). "Pushover analysis for asymmetric and setback multi-story buildings." *Proceedings of the 12th World Conf. on Earthquake Engng,* Auckland, New Zealand. Paper No. 1093.

[2] Fajfar P. (2002). "Structural analysis in earthquake engineering – A breakthrough of simplified nonlinear methods." *Proceedings of the 12th European Conf. on Earthquake Engng,* London, UK.

[3] Penelis G.G, and Kappos A.J. (2002). "3D pushover analysis: The issue of torsion." *Proceedings of the 12th European Conf. on Earthquake Engng,* London, UK.

[4] Chopra A. K, and Goel R. (2004). "A modal pushover analysis procedure to estimate seismic demands for unsymmetric-plan buildings." *Earthq. Engng and Struct. Dyn.*, 33: 903–927.

[5] Vamvatsikos D., and Cornell C. A. (2002). "Incremental dynamic analysis." *Earthq. Engng and Struct. Dyn.*, 31(3), 491-514.

[6] McKenna F., Fenves G. L., Jeremic B., and Scott M. H. 2000. Open system for earthquake engineering simulation (http://opensees.berkeley.edu).

[7] Mander J. B., Priestley M. J. N., and Park R. (1988). "Theoretical stress-strain model for confined concrete." *ASCE Journal of Struct. Engng*, 114(8): 1804–1826.

[8] Vamvatsikos D., and Cornell C. A. (2004). "Applied Incremental Dynamic Analysis." *Earthquake Spectra,* 20(2): 523–553.

[9] Vamvatsikos D., and Cornell C. A. (2005). "Developing efficient scalar and vector intensity measures for IDA capacity estimation by incorporating elastic spectral shape information." *Earthq. Engng and Struct. Dyn.*, (to appear).

[10] Hastie T. J., and Tibshirani R.J. (1990). *Generalized Additive Models*, Chapman & Hall, New York.